pISSN 1229-3008 eISSN 2287-6251
Progress in Superconductivity and Cryogenics
Vol. 26, No. 4, (2024), pp.83~88 https://doi.org/10.9714/psac.2024.26.4.083

Design of a small punch test apparatus for cryogenic environments using conduction cooling

Seungcheol Ryu[a], Yubin Kim[a], Seunggun Lee[b], and Seokho Kim[c,*]

[a] *Smart Manufacturing Engineering, Changwon National University, Republic of Korea*
[b] *Department of Hydrogen Materials Evaluation, Extreme Materials Institute Korea Institute of Materials Science, Republic of Korea*
[c] *Mechanical Engineering, Changwon National University, Republic of Korea*

(Received 13 December 2024; revised or reviewed 20 December 2024; accepted 21 December 2024)

Abstract

This study aims to design a Small Punch Test (SPT) apparatus for cryogenic environments using conduction cooling. SPT is a non-destructive testing method developed to evaluate material softening and embrittlement in applications such as power plants and fusion reactors. Compared to conventional tensile testing, SPT offers economic advantages in terms of miniaturization and repeatability. However, existing cryogenic SPT rely on liquid helium or evaporated helium gas, which involve high costs and inefficiency. In this study, a cryogenic cooling system utilizing a cryocooler was developed to eliminate the use of liquid helium, along with a rotary sample holder designed to enable testing of multiple specimens in a single cooling cycle. Key design considerations included minimizing external heat intrusion, optimizing thermal management of the load application structure, designing flexible copper connectors suitable for rotation, and applying multilayer insulation (MLI) to reduce radiative heat loads. In particular, the conduction cooling path was optimized to ensure that the specimen temperature could be stably maintained below 20 K, while minimizing displacement in the load application structure and enhancing thermal stability tailored to the characteristics of SPT. The proposed testing apparatus significantly improves cost efficiency and testing productivity compared to existing systems, and it is expected to set a new standard for material property evaluation in cryogenic environments.

Keywords: conduction cooling, cryogenic, material property evaluation, small punch test (SPT)

1. INTRODUCTION

The application of cryogenic environments has been expanding in recent years, particularly in technologies such as liquid hydrogen (LH_2), liquefied natural gas (LNG), and superconducting magnets [1, 2]. Consequently, the importance of evaluating material properties under cryogenic conditions has grown significantly. Liquid hydrogen has gained attention as an eco-friendly energy source with superior storage density. However, at its boiling point of 20 K, materials exhibit both high strength and brittleness, making accurate property evaluation under such conditions essential [3]. Evaluating the softening and embrittlement of materials in cryogenic environments is crucial for ensuring structural stability in applications such as power plants, aerospace, and hydrogen energy storage facilities [4].

Currently, widely used cryogenic property evaluation methods include boiling cooling systems employing liquid helium (4.2 K) and liquid nitrogen (77 K) [5]. However, these methods consume significant quantities of expensive cryogens during repetitive tests, particularly during specimen replacement and recooling processes, leading to increased costs. Additionally, boiling cooling systems operate reliably only at specific temperatures, making it difficult to establish continuous and variable temperature environments. The extended cooling time required in cryogenic environments further limits testing productivity compared to ambient temperature tests.

The Small Punch Test (SPT) is a non-destructive testing method that uses disk-shaped specimens approximately 6.5 mm in diameter and 0.5 mm in thickness to evaluate the mechanical properties of materials [6, 7]. SPT enables the evaluation of material properties on-site without compromising the structural integrity of components. By using miniature specimens, SPT offers economic advantages and is particularly suitable for assessing the properties of damaged components in the field. However, the development and standardization of SPT systems for cryogenic environments remain insufficient globally. There is a growing need for temperature-variable SPT systems capable of evaluating material properties under a wide range of conditions.

This study aims to develop an SPT apparatus employing conduction cooling using a cryocooler, replacing conventional liquid helium-based cooling systems and maximizing efficiency and testing productivity. To achieve this, a rotary sample holder was designed to enable the testing of multiple specimens in a single cooling cycle. The system also minimizes displacement in the load application structure to ensure high measurement precision during testing.

* Corresponding author: seokho@changwon.ac.kr

2. EXPERIMENTAL APPARATUS DESIGN

2.1. Design and Structure of Small Punch Tester with Conduction Cooling

The Small Punch Test (SPT) designed in this study is a material property evaluation device that can implement a variable temperature from 20 K, the saturation temperature of liquid hydrogen at atmospheric pressure, to 77 K, the saturation temperature of liquid nitrogen, through a conduction cooling method using a cryogenic refrigerator.

The tester design consists of a two-part structure in which the tester cryostat and the cryogenic refrigerator cryostat are separated, as shown in Fig. 1, to minimize the influence of the vibration of the cryogenic refrigerator on the evaluation results. The shape of the tester is compact, and the heat transfer path is optimized by arranging the cold head of the refrigerator facing upward and positioning it at the bottom of the tester cryostat.

In addition, the boiling cooling method operates stably only at a specific temperature, making it difficult to implement a continuous and variable temperature environment, and numerous cooling cycles in a cryogenic environment are the main causes of limiting test productivity.

2.2. Internal Structure of the Test Cryostat

The internal structure of the test cryostat incorporates a rotary jig system designed to enhance testing efficiency by enabling multiple experiments in a single cooling cycle. The system, as shown in Fig. 2, includes a sample holder mounted on a rotating jig plate that accommodates multiple specimens, enabling repeated tests at a single temperature or across multiple temperature points. The sample holder and specimens rotate together as a unit, while the base support, which holds the jig plate in place, is fixed to the cryostat.

Fig. 3 shows the detailed design of the rotary jig system, which builds upon the basic structure. The internal space of the test cryostat is maintained in a high vacuum state to prevent convective heat intrusion while operating under cryogenic conditions. To enable the rotation of the jig plate, a coupling structure was designed to connect the room temperature section and the cryogenic section, incorporating motion feedthrough mechanisms. This design ensures the vacuum seal within the cryostat while

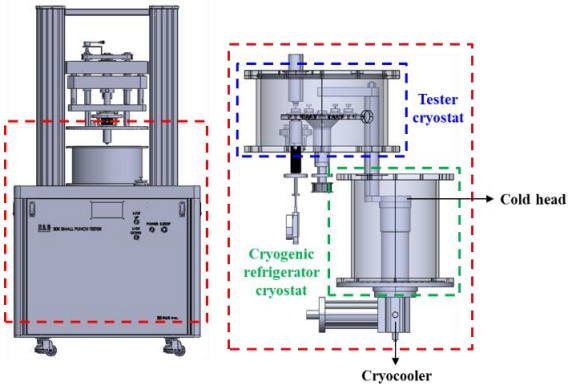

Fig. 1. Schematic design of the Small Punch Test (SPT) apparatus.

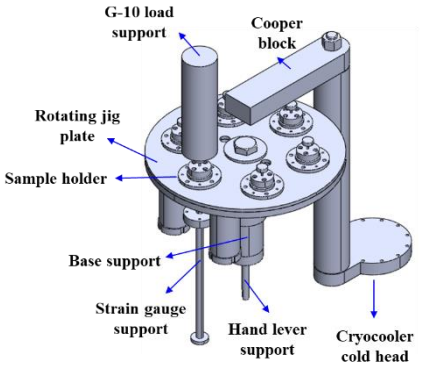

Fig. 2. Basic structure and key components of the rotary jig system.

allowing rotational movement.

Fig. 4 illustrates the force transmission structure of the tester, designed to maintain a high vacuum state within the cryostat while enabling precise force transmission to the specimen under cryogenic conditions. A bellows structure is employed to connect the room temperature section with the cryogenic section, with its lower flange secured to the tester cryostat and the upper flange connected to the load cell.

To reduce conductive heat intrusion from the room temperature components, G-10, a material with low thermal conductivity, is used for thermal insulation. However, the stiffness of the bellows can cause contraction, potentially misaligning the axis. To mitigate this, guide pins are installed between the flanges, ensuring stable vertical movement while preserving the internal vacuum.

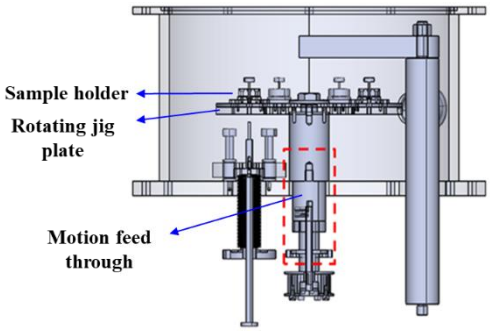

Fig. 3. Detailed design of the rotary jig system within the test cryostat.

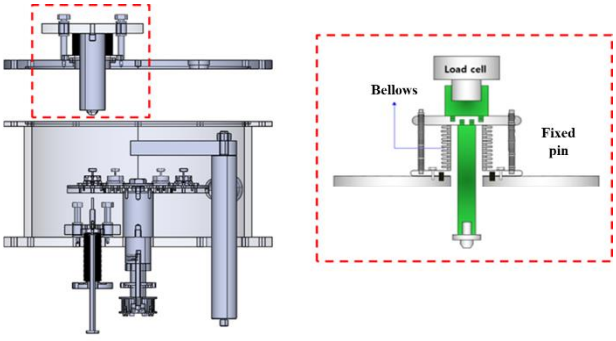

Fig. 4. Bellows-based force transmission design for cryogenic tester.

TABLE I
PARAMETERS USED FOR CALCULATING ROD AREA [8]

Parameter	Value	Unit
STS 316L modulus ($E_{specimen}$)	185	GPa
G-10 modulus (E_{rod})	18	GPa
Rod area	1,816 ↑	mm^2

Minimizing conductive heat intrusion from the room temperature section to the load cell is achieved by using G-10 material, which has low thermal conductivity. The cross-sectional area of the G-10 rod must be designed to match the load capacity of the tester.

In this study, the diameter of the G-10 rod was calculated based on the assumption that the deformation of G-10 under the same stress is limited to 1% of the deformation of a Stainless-steel 316L specimen. Using the following (1), the required cross-sectional area of the G-10 rod was determined, where σ represents stress, F is the applied load, E is Young's modulus, A is the cross-sectional area, and ϵ is the strain.

$$\sigma = E\epsilon \;\rightarrow\; F = AE\epsilon$$

$$A_{rod}E_{rod}\epsilon_{rod} = A_{specimen}E_{specimen}\epsilon_{specimen}$$

$$A_{rod} = \frac{A_{specimen}E_{specimen}\epsilon_{specimen}}{E_{rod}\epsilon_{rod}}$$

$$\epsilon_{rod} = 0.01 \times \epsilon_{specimen}$$

$$A_{rod} = \frac{A_{specimen}E_{specimen}\epsilon_{specimen}}{E_{rod}(0.01 \times \epsilon_{specimen})} \quad (1)$$

The detailed material properties used in (1) are presented in Table I. According to the calculations, the minimum cross-sectional area of the G-10 rod is 1,816 mm^2, and if the G-10 rod has a circular shape, its diameter must exceed 24 mm. In this system, the diameter of the G-10 rod was selected to be 25 mm to minimize conductive heat load.

Fig. 5 illustrates the structural design for measuring the displacement of a specimen subjected to force from the load cell. In the Small Punch Test (SPT), a strain gauge is attached to the lower section of the specimen, where fracture occurs, to measure the inherent deformation of the specimen. The strain gauge operates at room temperature while minimizing conductive heat intrusion from internal structures.

The structure employs a bellows mechanism combined with a flange to connect the room temperature and cryogenic sections. The upper flange of the bellows is fixed to the tester cryostat, maintaining a high vacuum and cryogenic environment outside the bellows. Specimen displacement is transmitted through the specimen-bellows connecting rod, as shown in Fig. 5, to the strain gauge support and measured by the strain gauge.

The specimen-bellows connecting rod and strain gauge support are also made of G-10 material, selected for their mechanical strength and low thermal conductivity. The required G-10 cross-sectional area is calculated similarly to the load cell part to ensure sufficient strength. Due to the inherent spring stiffness of the bellows, the deformation caused by this stiffness must be subtracted from the measured displacement during material property evaluation to ensure accuracy in the displacement measurements.

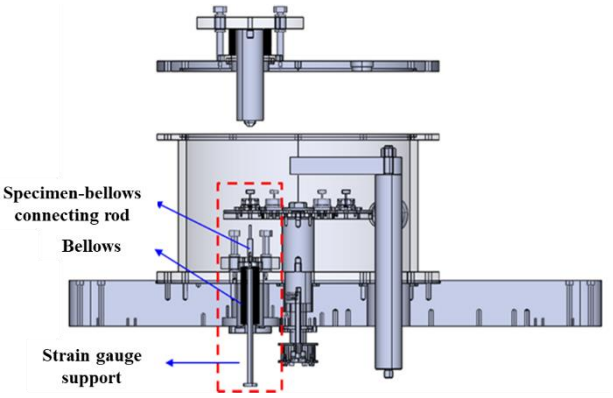

Fig. 5. Structural design of the displacement measurement system in the tester.

2.3. Thermal Design of the Tester Cryostat

The cooling mechanism and scenario for the specimen were designed considering the conduction cooling method. The copper block, attached to the cold head of the cryocooler, is connected to the tester cryostat through a bellows passage. To cool the specimen at the center of the rotary jig plate, a dedicated cooling structure using oxygen-free copper braided wire derived from the copper block was proposed. Fig. 6 illustrates the structure designed to cool the internal components of the tester cryostat via the copper block. Since the rotary jig plate, made of stainless steel, has low thermal conductivity, a thin copper plate was attached to enhance conduction heat transfer. The copper braids extend from the copper block to the copper plate and the G-10 rod connected to the tester load cell.

Thermal loads associated with the tester structure were analyzed, primarily considering three factors: conduction heat intrusion, convective heat load, and radiative heat load. Conduction heat intrusion occurs through internal structures connected to the room temperature section. Convective heat load is eliminated via vacuum insulation,

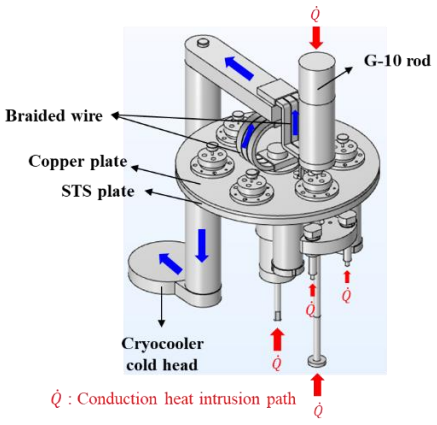

Fig. 6. Internal cooling path and heat transfer model of the tester.

while radiative heat load is reduced through the application of radiation shields. An optimized cryogenic support structure was designed to minimize the overall thermal load.

Fig. 7 illustrates the thermal properties of G-10 material, highlighting its exceptional suitability for cryogenic applications [8]. At cryogenic temperatures, G-10 exhibits significantly lower thermal conductivity compared to metal alloys while maintaining excellent mechanical properties at both room and cryogenic temperatures [9]. These attributes make G-10 an ideal material for reducing conductive heat intrusion and ensuring structural stability when combined with appropriately designed connections to metal alloys.

Convective heat intrusion is effectively mitigated by the vacuum insulation structures incorporated into the tester and cryocooler cryostats. As shown in Fig. 8, the thermal conductivity of air decreases significantly under high vacuum conditions, specifically at 10^{-3} torr. By using a turbo pump to achieve a vacuum level of 10^{-5} torr, convective heat intrusion can be rendered negligible, ensuring the thermal stability of the system.

Radiative heat intrusion, calculated using (2), becomes a critical factor due to the significant temperature difference between room temperature (300 K) and cryogenic temperatures (20 K) [11, 12].

$$\dot{Q}_{rad} = \epsilon \sigma A_s (T_h^4 - T_c^4) \quad (2)$$

Here, ϵ is the emissivity, σ is the Stefan-Boltzmann constant, A_s is the surface area, T_h is the temperature of the high-temperature section, and T_c is the temperature of the low-temperature section. To minimize radiative heat load, multi-layer insulation (MLI) with high reflectivity was employed. The system utilizes 30 layers of MLI, designed to reduce the radiative heat intrusion. Using (3) and the parameters in Table II, the resulting radiative heat load was calculated to be $q_{rad} = 5\ W/m^2$.

$$\dot{Q}_{N\ shield} = \frac{A_s \sigma \Delta T^4}{(N+1)\left(\frac{1}{\epsilon_1} + \frac{1}{\epsilon_2} - 1\right)} = \frac{1}{N+1} \dot{Q}_{no\ shield} \quad (3)$$

Where N represents the number of MLI layers, and ϵ_1 and ϵ_2 denote the emissivities of the reflective surfaces. These design measures collectively ensure efficient thermal management in the cryogenic testing system.

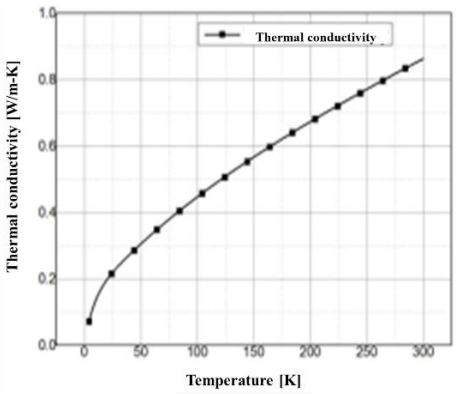

Fig. 7. G-10 thermal conductivity.

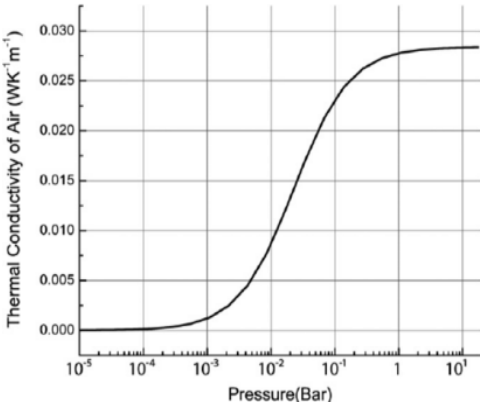

Fig. 8. Thermal conductivity according to vacuum [10].

3. THERMAL ANALYSIS OF SPT UTILIZING CONDUCTION COOLING METHOD

The thermal boundary conditions for the analysis were based on the conductive, radiative, and convective heat intrusion factors described earlier. Additionally, the cooling capacity of the cryocooler was considered by applying the performance curve of the ULVAC Cryogenics RSC 40T cryocooler, as shown in Fig. 9. The temperature distribution and thermal loads were evaluated using the COMSOL Multiphysics simulation software.

3.1. Temperature Distribution and Thermal Load Optimization Results

The thermal analysis results of the SPT utilizing the conduction cooling method are illustrated in Fig. 10, showing the temperature distribution from the cryocooler cold head to the interior of the tester cryostat. After performing 3D thermal analysis, the measured thermal loads revealed 2 W of radiative heat intrusion and 12 W of conductive heat intrusion, resulting in a total thermal load of approximately 14 W. The detailed dimensions of the braid wires used for cooling are presented in Table III.

Fig. 11 illustrates the temperature distribution of key thermal load areas in the SPT utilizing the conduction cooling method. After performing a 3D thermal analysis, the cross-sectional temperature distribution was observed. The minimum temperature of the rotating jig plate was found to be 19 K. Additionally, the temperature at the end of the copper block was measured at 15.5 K, indicating a temperature difference of approximately 3.5 K between the rotating jig plate and the copper block.

TABLE II
TYPICAL VALUES OF RADIATIVE HEAT FLUX [13]

Material	$T_h \rightarrow T_c$ [K]	N	q_r [mW/m^2]
Superinsulation (MLI)	20 → 4	≤ 10	2
	80 → 20	40	40
	300 → 80	60	2,500

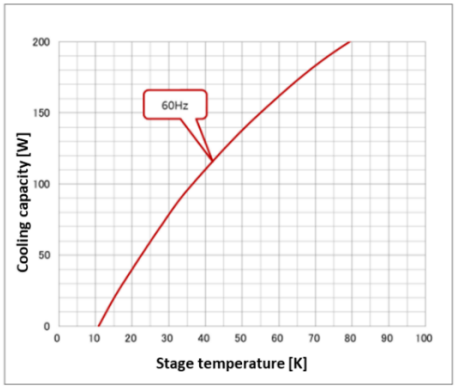

Fig. 9. Cryocooler performance curve.

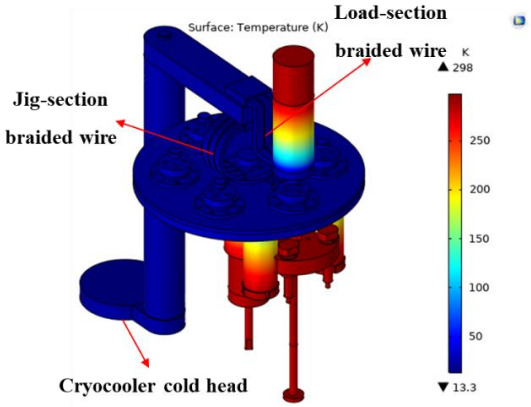

Fig. 10. SPT temperature distribution.

Fig. 12 illustrates the temperature distribution around the specimen. After conducting a 3D thermal analysis, the cross-sectional temperature distribution was observed. The minimum temperature of the specimen was found to be 19.5 K, meeting the target minimum temperature of 20 K. Additionally, the temperature at the load section was measured at 23.3 K, indicating a temperature difference of approximately 3.8 K between the load section and the specimen. Furthermore, while a noticeable temperature difference was observed near the strain gauge support below the specimen, the associated thermal load was less than 0.1 W, confirming that it has a negligible effect on the specimen temperature.

TABLE III
THERMAL LOAD AND BRAIDED WIRE SPECIFICATIONS FOR SPT SYSTEM

Parameter	Value	Unit
Load-section braided wire cross-sectional area	396 (33 mm × 6 mm × 2 ea)	mm^2
Load-section braided wire length	100	mm
Jig-section braided wire cross-sectional area	198 (33 mm × 6 mm × 1 ea)	mm^2
Jig-section braided wire length	110	mm
Radiative heat load ($\dot{Q}_{rad}$)	2	W
Conductive heat load ($\dot{Q}_{cond}$)	12	W
Total heat load ($\dot{Q}_{total}$)	14	W

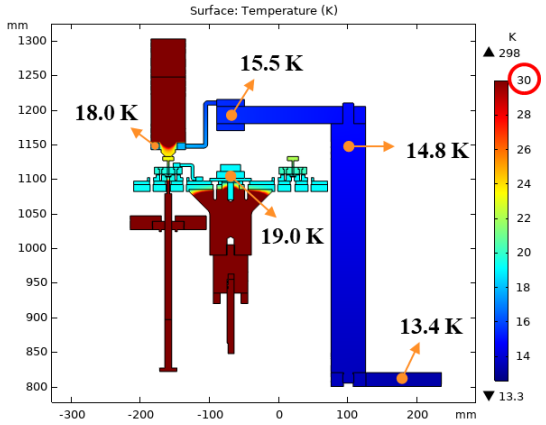

Fig. 11. Cross-sectional temperature distribution of key thermal load areas.

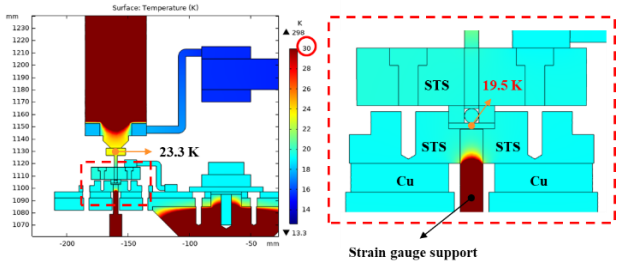

Fig. 12. Cross-sectional temperature distribution around the specimen.

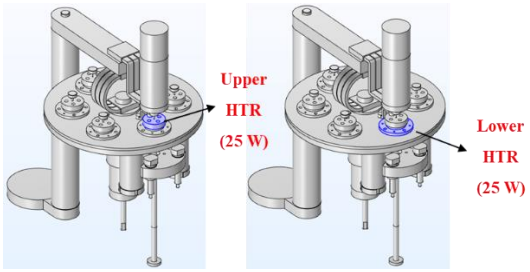

Fig. 13. Heater installation positions: Upper and Lower of Specimen.

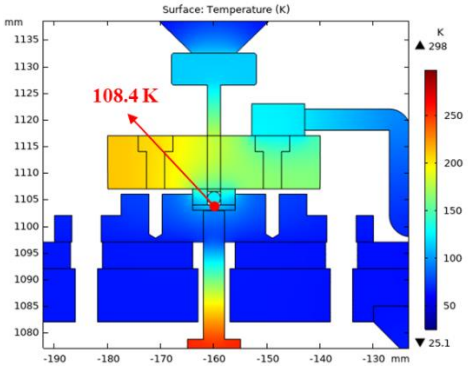

Fig. 14. Cross-sectional temperature distributions based on heater power .

3.2. Variable Temperature Control for Specimen Testing

In this system, two heater placement strategies were evaluated: near the cryocooler cold head for overall system control and near the specimen for direct temperature

control. Considering the long cooling path, the specimen-focused placement was selected for its ability to ensure precise and consistent thermal conditions.

Figs. 13 and 14 illustrate the heater positions and the corresponding temperature distributions when 25 W of heat was applied to each heater. Without heating, the specimen temperature was maintained at 19 K, while heating raised it to 108 K. These results demonstrate the system's capability to achieve the desired temperature range, encompassing the boiling points of liquid hydrogen (20 K) and liquid nitrogen (77 K), essential for cryogenic applications.

4. CONCLUSION

In this system This study successfully designed a small punch test (SPT) apparatus for cryogenic environments utilizing conduction cooling and demonstrated its ability to achieve a stable target temperature below 20 K. Through optimized designs, including G-10 support rods, oxygen-free copper braided wires, and multi-layer insulation (MLI), the total thermal load was minimized to approximately 14 W, effectively reducing conductive and radiative heat intrusion. Additionally, by implementing heaters near the specimen, variable temperature control was achieved, ranging from 19 K to 108 K, meeting the critical temperature requirements for cryogenic applications, including the boiling points of liquid hydrogen (20 K) and liquid nitrogen (77 K).

The rotary jig system significantly improved testing productivity by enabling multiple specimen tests within a single cooling cycle. The system is optimized for cost efficiency and thermal stability, offering a new standard for material property evaluations in diverse cryogenic applications. Future studies will focus on enhancing the precision of temperature control systems and further reducing thermal loads through improved design and additional performance validation.

ACKNOWLEDGMENT

This work was supported by the Fundamental Research Program (PNK 9340) of the Korea Institute of Materials Science (KIMS).

REFERENCES

[1] M. Aasadnia and M. Mehrpooya, “Large-scale liquid hydrogen production methods and approaches: A review,” *Appl. Energy*, vol. 212, pp. 57-83, 2018.

[2] H. M. Chang, B. H. Kim, and B. Choi, “Hydrogen liquefaction process with Brayton refrigeration cycle to utilize the cold energy of LNG,” *Cryogenics*, vol. 108, pp. 103093, 2020.

[3] Y. Qiu, H. Yang, L. Tong, and L. Wang, “Research progress of cryogenic materials for storage and transportation of liquid hydrogen,” *Metals*, vol. 11, no. 7, pp. 1101, 2021.

[4] Z. Sápi and R. Butler, “Properties of cryogenic and low temperature composite materials–A review,” *Cryogenics*, vol. 111, pp. 103190, 2020.

[5] A. N. Pavlenko and D. V. Kuznetsov, “Development of methods for heat transfer enhancement during nitrogen boiling to ensure stabilization of HTS devices,” *J. Eng. Thermophys*., vol. 30, no. 4, pp. 526-562, 2021.

[6] T. E. García, B. Arroyo, C. Rodríguez, F. J. Belzuence, and J. A. Á lvarez, “Small punch test methodologies for the analysis of the hydrogen embrittlement of structural steels,” *Theor. Appl. Fract. Mech.*, vol. 86A, pp. 89-100, 2016.

[7] R. J. Lancaster, S. P. Jeffs, B. J. Haigh, and N. C. Barnard, “Derivation of material properties using small punch and shear punch test methods,” *Mater. Des*., vol. 215, pp. 110473, 2022.

[8] “G-10 CR Fiberglass Epoxy,” *National Institute of Standards and Technology*, Accessed: Oct. 25, 2024, [Online]. Available: https://trc.nist.gov/cryogenics/materials/G-10%20CR%20Fiberglass%20Epoxy/G10CRFiberglassEpoxy_rev.htm.

[9] Y. Iwasa, “Case studies in superconducting magnets: design and operational issues,” *Springer*, pp. 638, 2009.

[10] G. R. Barron and G. F. Nellis, “Cryogenic heat transfer,” *CRC Press*, pp. 47, 2017.

[11] E. M. Sparrow, “Radiation heat transfer,” *Routledge*, 2018.

[12] Y. Iwasa, “Case studies in superconducting magnets: design and operational issues,” *Springer*, pp. 250, 2009.

[13] Y. Iwasa, “Case studies in superconducting magnets: design and operational issues,” *Springer*, pp. 249, 2009.